

Improved Deep-Red Phosphorescence in Cyclometalated Iridium Complexes via Ancillary Ligand Modification

Evanta Kabir, Steven Sittel, Boi-Lien Nguyen, and Thomas S. Teets*^[a]

Abstract: In this work, we describe bis-cyclometalated iridium complexes with efficient deep-red luminescence. Two different cyclometalating (C[^]N) ligands—1-phenylisoquinoline (piq) and 2-(2-pyridyl)benzothiophene (btp)—are used with six strong π -donating ancillary ligands (L[^]X) to furnish a suite of 10 new complexes with the general formula Ir(C[^]N)₂(L[^]X). Improvements in deep-red photoluminescence quantum yields were accomplished by the incorporation of sterically encumbering substituents onto the ancillary ligand, which can enhance the radiative rate constant (k_r) and/or reduce the non-radiative rate constant (k_{nr}). Five of the complexes were characterized by X-ray crystallography, and all of them were investigated by in-depth spectroscopic and electrochemical measurements.

Introduction

Luminescent cyclometalated iridium(III) complexes have become one of the most prominent classes of molecular phosphors, contributing to numerous applications in photocatalysis,^[1–3] bioimaging, and sensing,^[4,5] and most notably, organic light-emitting diodes (OLEDs)^[6–9] and light-emitting electrochemical cells.^[10,11] These compounds luminesce from triplet excited states with ligand-centered (³LC or ³ $\pi\pi^*$) and metal-to-ligand charge transfer (³MLCT or ³d π^*) character, mixing through configuration interaction. Homoleptic complexes of the type *fac*-Ir(C[^]N)₃ (C[^]N = cyclometalating ligand) are popular in both OLED and photocatalysis applications,^[1,12,13] and heteroleptic complexes of type Ir(C[^]N)₂(L[^]X) (L[^]X = ancillary ligand) have also become prominent. The ancillary ligands in the heteroleptic complexes can strongly influence the emission color,^[14,15] but most often shift redox potentials (especially the formally Ir^{IV}/Ir^{III} couple) and perturb the excited state dynamics, while only subtly influencing the photoluminescence spectrum.^[16,17]

Facile color tunability, highly photoluminescence quantum yields (Φ_{PL}), and relatively short phosphorescence lifetimes (τ) are some of the key features of cyclometalated iridium(III) complexes, which along with their good thermal and photostability lead to applications in diverse fields. There are many examples of iridium(III) complexes which emit in the blue to orange regions of the spectrum with near unity quantum yields,^[18–22] but red and near-infrared emitters in the lower-energy regions of the spectrum typically have lower quantum yields, which is an important performance metric to function in commercial devices. The

quantum yield (Φ_{PL}) is the ratio of the radiative rate constant (k_r) to the sum of radiative and non-radiative (k_{nr}) rate constants. According to the energy gap law,^[23,24] the non-radiative rate constant (k_{nr}) increases for complexes with lower-energy excited states, on account of greater vibrational overlap between the ground and excited states.^[25] On the other hand, the radiative rate (k_r) has a cubic dependence on the transition energy and is expected to be smaller when longer emission wavelengths are accessed.^[6] The radiative rate constant k_r has a strong dependence on the spin-orbit coupling (SOC) in the excited state, which derives exclusively from the MLCT states that contribute to the emissive triplet state, T₁. The excited-state MLCT character is sensitive to the nature of the ancillary ligand in heteroleptic bis-cyclometalated iridium complexes, so synthetic strategies which augment the MLCT character can lead to increases in k_r and improvements in Φ_{PL} .

Using the above insights, our group has made significant advances in the performance of cyclometalated iridium complexes which emit in the low-energy regions of the visible spectrum. Our strategy involves the incorporation of nitrogen-donor, electron-rich ancillary ligands into heteroleptic Ir(C[^]N)₂(L[^]X) complexes. We have shown that this strategy can lead to significant improvements in the photoluminescence quantum yields of yellow-orange^[17] and red-emitting^[26] compounds, with quantum yields as high as 0.8 for the red emitters. Subsequent work on related compounds revealed additional structure-property relationships in these red-emitting compounds, showing how the ancillary ligand structure (chelate ring-size, donor atoms, and substituents) influenced the nature of the excited state and the excited-state dynamics.^[27] One finding from these studies is that when the cyclometalated aryl group is a simple phenyl ring, as is the case for red-emitting compounds where C[^]N = 1-phenylisoquinoline (piq), the photoluminescence wavelength is very sensitive to the electron-richness of the ancillary ligand, leading to deep-red luminescence (defined here as $\lambda_{max} > 650$ nm) for some ancillary ligands. For example, the complex Ir(piq)₂(dipba) (dipba = N,N-diisopropylbenzamidinate) has a photoluminescence λ_{max} of 671 nm in room-temperature THF solution, with a respectable quantum yield of 0.34.^[26,27] That said, the two deep-red emitters we prepared in these previous works had k_r values that were smaller and, particularly evident, k_{nr} values that were larger than the structurally related compounds that phosphoresce in the red region, limiting their quantum yields to fairly modest values. Further improvements in the quantum yields require synthetic strategies capable of augmenting the k_r values and/or decreasing the k_{nr} values for compounds which emit in the deep red portion of the spectrum.

In this work we present synthetic modifications that lead to improved deep-red-emitting cyclometalated iridium complexes. Two key findings of this report are (i) sterically encumbering substituents on the electron-rich ancillary ligand can lead to significant improvements in Φ_{PL} for deep-red phosphors, and (ii) making the ancillary ligand even more electron rich can shift the photoluminescence to the near-infrared (NIR) region, $\lambda_{max} > 700$ nm. Our work here describes a suite of ten heteroleptic bis-

[a] Dr. E. Kabir, S. Sittel, B.-L. Nguyen, and Prof. Thomas S. Teets
Department of Chemistry
University of Houston
Lamar Fleming Jr. Building, 3585 Cullen Blvd. Room 112
Houston, TX 77204-5003
E-mail: tteets@uh.edu

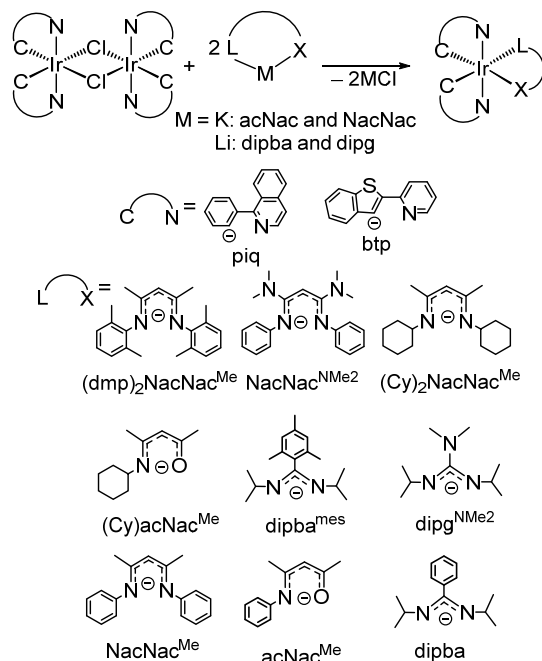
Supporting information for this article is given via a link at the end of the document

cyclometalated iridium complexes, prepared by pairing the cyclometalating ligands piq and btp with six new ancillary ligands. This work provides further insight into the influence of the ancillary ligand structure on the electrochemical and photophysical properties, highlighting the effects of replacing *N*-aryl substituents with alkyl groups, and of augmenting the steric profile of the ancillary ligand. Significantly, in a few of the compounds the modifications to the ancillary ligand lead to increases in k_r and/or decreases in k_{nr} relative to structurally related compounds, producing deep-red emitters with photoluminescence quantum yields among the highest reported to date.

Results and Discussion

Synthesis of heteroleptic iridium complexes. The general synthetic procedure for the ten new complexes of type $\text{Ir}(\text{C}^{\wedge}\text{N})_2(\text{L}^{\wedge}\text{X})$ ($\text{C}^{\wedge}\text{N}$ = 1-phenylisoquinoline (piq) and 2-(2-pyridyl)benzothiophene (btp)) is described in Scheme 1. These two cyclometalating ligands are paired with six different electron-rich ancillary ligands to prepare the new compounds described here, and Scheme 1 also summarizes three reference $\text{Ir}(\text{piq})_2(\text{L}^{\wedge}\text{X})$ compounds, **R1–R3**, which will be frequently referred to in this paper. In previous research we have extensively worked with *N*-phenyl-substituted β -diketiminate ($\text{NacNac}^{\text{Me}}$) and β -ketoiminate (acNac^{Me}) ancillary ligands.^[17,26,28,29] To increase the steric profile we introduced methyl substituents at the *ortho* positions of the *N*-aryl in $(\text{dmp})_2\text{NacNac}^{\text{Me}}$. Modifications to make the ancillary ligand more electron-rich include replacing backbone methyl groups with dimethylamino substituents ($\text{NacNac}^{\text{NMe}_2}$), or replacing the *N*-phenyl substituents with cyclohexyl rings in $(\text{Cy})_2\text{NacNac}^{\text{Me}}$ and $(\text{Cy})\text{acNac}^{\text{Me}}$. Similarly, we^[26,27] and others^[30–32] have used an amidinate ancillary ligand (dipba) in the design of bis-cyclometalated iridium complexes, and here we incorporate modifications to make the amidinate more sterically encumbered ($\text{dipba}^{\text{mes}}$), or make it more electron-rich by changing to a guanidinate ($\text{dipg}^{\text{NMe}_2}$). The numbering scheme uses numerical designators for each $\text{C}^{\wedge}\text{N}$ ligand (piq = **1**, and btp = **2**), with letters (**a–f**) denoting each $\text{L}^{\wedge}\text{X}$ ligand. To prepare the complexes, the chloro-bridged dimers $[\text{Ir}(\text{C}^{\wedge}\text{N})_2(\mu\text{-Cl})_2]$ were treated with $(\text{dmp})_2\text{NacNac}^{\text{Me}}\text{K}$ or $\text{NacNac}^{\text{NMe}_2}\text{K}$ at room temperature in THF to afford complexes **1a–b** and **2a–b** in moderate yields. A slightly different method was used to obtain complexes **1c–d** and **2c–d**, where the chloro-bridged dimers were treated with the in situ-generated lithium salt of $\text{dipba}^{\text{mes}}$ and $\text{dipg}^{\text{NMe}_2}$ in tetrahydrofuran (THF) at 85 °C, whereas for **1e–f** the piq-ligated dimer was treated with $(\text{Cy})_2\text{NacNac}^{\text{Me}}\text{K}$ or $(\text{Cy})\text{acNac}^{\text{Me}}\text{K}$ in toluene at 130 °C. The identity and the bulk purity of the complexes were confirmed by ^1H and $^{13}\text{C}\{^1\text{H}\}$ NMR.

The NMR spectra evinced C_2 symmetry for all complexes except **1f**, where asymmetric $(\text{Cy})\text{acNac}$ ancillary ligand results in a C_1 point group, giving rise to distinct NMR resonances for each proton and carbon nucleus. All NMR spectra show the presence



Compounds new to this work:

1a: $\text{C}^{\wedge}\text{N}$ = piq, $\text{L}^{\wedge}\text{X}$ = $(\text{dmp})_2\text{NacNac}^{\text{Me}}$

1b: $\text{C}^{\wedge}\text{N}$ = piq, $\text{L}^{\wedge}\text{X}$ = $\text{NacNac}^{\text{NMe}_2}$

1c: $\text{C}^{\wedge}\text{N}$ = piq, $\text{L}^{\wedge}\text{X}$ = $\text{dipba}^{\text{mes}}$

1d: $\text{C}^{\wedge}\text{N}$ = piq, $\text{L}^{\wedge}\text{X}$ = $\text{dipg}^{\text{NMe}_2}$

1e: $\text{C}^{\wedge}\text{N}$ = piq, $\text{L}^{\wedge}\text{X}$ = $(\text{Cy})_2\text{NacNac}^{\text{Me}}$

1f: $\text{C}^{\wedge}\text{N}$ = piq, $\text{L}^{\wedge}\text{X}$ = $(\text{Cy})\text{acNac}^{\text{Me}}$

2a: $\text{C}^{\wedge}\text{N}$ = btp, $\text{L}^{\wedge}\text{X}$ = $(\text{dmp})_2\text{NacNac}^{\text{Me}}$

2b: $\text{C}^{\wedge}\text{N}$ = btp, $\text{L}^{\wedge}\text{X}$ = $\text{NacNac}^{\text{NMe}_2}$

2c: $\text{C}^{\wedge}\text{N}$ = btp, $\text{L}^{\wedge}\text{X}$ = $\text{dipba}^{\text{mes}}$

2d: $\text{C}^{\wedge}\text{N}$ = btp, $\text{L}^{\wedge}\text{X}$ = $\text{dipg}^{\text{NMe}_2}$

Reference compounds:

R1: $\text{C}^{\wedge}\text{N}$ = piq, $\text{L}^{\wedge}\text{X}$ = $\text{NacNac}^{\text{Me}}$

R2: $\text{C}^{\wedge}\text{N}$ = piq, $\text{L}^{\wedge}\text{X}$ = acNac^{Me}

R3: $\text{C}^{\wedge}\text{N}$ = piq, $\text{L}^{\wedge}\text{X}$ = dipba

Scheme 1. Synthesis of bis-cyclometalated iridium complexes.

of single product in each case, confirming the absence of any isomeric complexes in the isolated products.

Structural characterization by X-ray crystallography.

Complexes **1c**, **1d**, **2a**, **2b**, and **2d** were characterized by single crystal X-ray diffraction, with the structures depicted in Figures 1 and S1, and detailed crystallographic data are reported in Tables S1–S2. Single crystals were grown via vapor diffusion of pentane into dichloromethane or tetrahydrofuran solution or by layering pentane onto a dichloromethane solution at room temperature inside the glovebox. The iridium center is found to be at the center of a distorted octahedral geometry in all of the characterized structures and the expected trans disposition of the two nitrogen atoms of the cyclometalating ligands is observed. Excepting

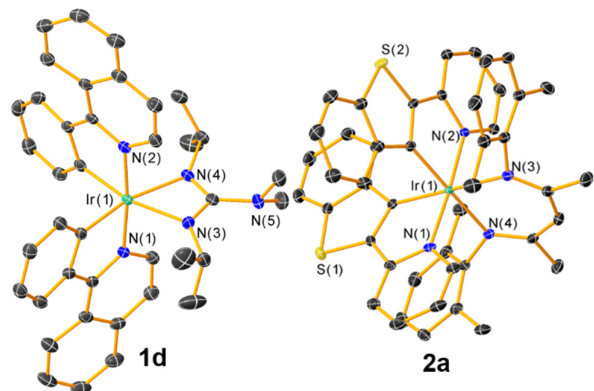


Figure 1. Molecular structures of complexes **1d** and **2a**, determined by single-crystal X-ray diffraction. Ellipsoids are depicted at 50% probability with hydrogen atoms and solvent molecules.

NacNac^{NMe2} complex **2b**, where the NacNac core is "buckled" in a fashion analogous to other structurally characterized NacNac^{NMe2} complexes from our group,^[28,29] the ancillary ligand core and the chelated iridium atom are planar. The C–O, C–N, and C–C bond distances of the ancillary ligand chelate rings in all five characterized complexes are intermediate between typical single- and double-bond distances, suggesting a π -delocalized core. Unsurprisingly, the structure of the ancillary ligand determines the ancillary ligand N–C–N bite angle, which averages 60.49(10)° for complexes **1c**, **1d**, and **2d**, and is much larger in NacNac complexes **2b** is (85.26(7)°) and **2a** (90.27(10)°).

The synthetic modifications we have made in this work, in an effort to make the ancillary ligands more sterically encumbered and/or more electron-rich, generally had only subtle effects on solid-state structural metrics. For example, (dmp)₂NacNac^{Me} complex **2a** shows a close approach of both N-aryl groups to a nearby Ir-aryl, in a nearly eclipsed orientation with apparent π - π stacking between the rings. This type of structural motif was also observed in several other iridium NacNac complexes previously described by our group, which lacked the *ortho*-methyl substituents.^[17,33] In addition, comparison of previously reported Ir(btp)₂(dipba)^[26] with complex **1c** shows that increased steric bulk on the amidinate's central aryl ring exerts only subtle influences on the structure. One small difference between these structures is an increase in the dihedral angle between the backbone aryl ring and the mean plane of the four-member chelate ring, which increases from 70.75° in the dipba complex to 81.58° in the mesityl-substituted complex **1c**. Similarly, the addition of electron-donating groups in dipg^{NMe2} complexes **1d** and **2d** does not demonstrably perturb the structures relative to the analogous amidinate complexes.

Electrochemical Properties. Figures 2 and S2 display overlaid cyclic voltammograms of the complexes, arranged by C^{*}N ligands, and their results are summarized in Table 1. Redox potentials are reported relative to the ferrocenium/ferrocene couple. All the

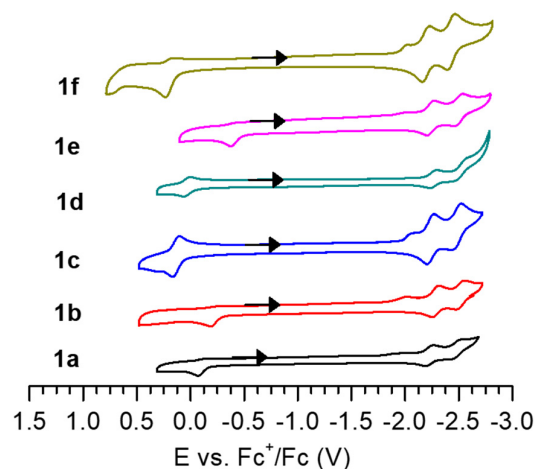


Figure 2. Overlaid cyclic voltammograms of complexes **1a-f**. CVs were recorded in acetonitrile with 0.1 M NBu₄PF₆ supporting electrolyte, using a glassy carbon working electrode and a scan rate of 0.1 V/s. The arrows indicate the scan direction. Concentrations were not carefully controlled, and currents are low in some of plots because of the limited solubility of some of the compounds in acetonitrile.

complexes described in this work display a formally Ir^{IV}/Ir^{III} redox couple (E^{ox}), with potentials that are strongly dependent on the identity of the ancillary ligand. Complexes supported by (dmp)₂NacNac^{Me}, **1a** and **2a**, have similar oxidation potentials (E^{ox} = -0.07 V and +0.06 V, respectively), close to the ferrocenium/ferrocene couple. The electron-donating backbone dimethylamino groups in complexes **1b** and **2b** make the molecules easier to oxidize, with potentials that are cathodically shifted by at least 120 mV. Addition of dimethylamino substituents in dipg^{NMe2} complexes **1d** and **2d** resulted in a cathodic shift of 110 mV when comparing to the amidinate complexes **1c** and **2c**. The largest effect on the redox potential was realized by replacing the NacNac *N*-aryl groups with the cyclohexyl groups, resulting in an oxidation potential for complex **1e** of -0.37 V. This observation is in line with a previously reported (Cy)₂NacNac complex from our group, Ir(ppy)₂((Cy)₂NacNac) (ppy = 2-phenylpyridine), which had a nearly identical value for E^{ox} and shows that the basicity of the chelated nitrogen atoms can strongly influence the HOMO energy. Another clear trend, which we have previously noted in other related complexes,^[26,27] is that compounds with the smaller N–C–N bite angle, **1c/d** and **2c/d**, were more difficult to oxidize than the NacNac complexes. Finally, complex **1f** (E^{ox} = +0.24 V) with a mixed *N,O* (Cy)acNac^{Me} chelate, was the most difficult to oxidize of the complexes in the piq series, and the reported potential is quite similar to the previously reported *N*-phenyl substituted complex Ir(piq)₂(acNac^{Me}) (**R2**),^[26] suggesting that for the acNac ancillary ligand the basicity of the nitrogen donor is less important in determining HOMO energies and associated redox potentials than it is in the NacNac series. To summarize, the trends in E^{ox} values indicate that the energy of the HOMO is

strongly determined by the nature of the ancillary ligand, with associated redox potentials that span a wide range of >0.5 V.

Table 1. Summary of cyclic voltammetry data for Ir(piq)₂(L^{AX}) complexes **1a–f**

C ^{AN} = piq (1)	(E vs. Fc ^{+/0} /Fc) / V ^[a]	
	E ^{red}	E ^{ox}
L ^{AX} = (dmp) ₂ NacNac ^{Me} (1a)	-2.22, -2.48	-0.07 ^[b]
L ^{AX} = NacNac ^{Me2} (1b)	-2.28, -2.52	-0.19 ^[b]
L ^{AX} = dipba ^{Me3} (1c)	-2.24, -2.48	+0.14
L ^{AX} = dipg ^{NMe2} (1d)	-2.26, -2.59 ^[b]	+0.03
L ^{AX} = (Cy) ₂ NacNac ^{Me} (1e)	-2.24, -2.50	-0.37 ^[b]
L ^{AX} = (Cy)acNac ^{Me} (1f)	-2.20, -2.42	+0.24 ^[b]

C ^{AN} = btp (2)		
L ^{AX} = (dmp) ₂ NacNac ^{Me} (2a)	-2.58 ^[b]	0.06 ^[b]
L ^{AX} = NacNac ^{Me2} (2b)	-2.62 ^[b]	-0.17
L ^{AX} = dipba ^{Me3} (2c)	-2.57 ^[b]	0.23
L ^{AX} = dipg ^{NMe2} (2d)	-2.60 ^[b]	0.12

[a] Experiments were performed in acetonitrile solvent with 0.1 M NBu₄PF₆ electrolyte with scan rate of 0.1 V/s using a glassy carbon working electrode and a silver wire pseudo-reference electrode. Potentials are referenced against the ferrocene/ferrocenium redox couple. [b] Observed wave is irreversible, and the respective E_{p,c} or E_{p,a} peak potential is reported.

The reduction potentials (E^{red}) of the new complexes described here depend only slightly on the identity of the L^{AX} ligands. The two observed waves for the piq complexes are associated with sequential population of a π* orbital on each C^{AN} ligand, with measured potentials beyond -2.0 V. We do note a minor “pre-feature” wave near -2.0 V in most complexes, which arises irrespective of scan direction and we think can be attributed to the poor solubility in acetonitrile upon reduction, causing some deposition onto the electrode. As such the reported E^{red} values are for the one or two clearly-resolved waves that occur beyond this minor pre-feature. Consistent with this notion, this pre-feature wave was mostly absent when the CVs of complexes **1a–1c** were recorded in THF, as shown in Figure S3 of the Supporting Information. The first reduction potentials for all piq-ligated complexes were reversible, ranging from -2.20 V to -2.28 V. Another subsequent reduction wave was observed for complexes **1a–f**, with potentials ranging between -2.42 (**1f**) and -2.59 (**1d**) V, reversible in most cases. All btp-ligated complexes display only

one clearly-resolved reduction wave at a more negative potential than the piq series. In contrast to the HOMO energies, which are very dependent on the structure of the ancillary ligand, the observed reduction potentials of the new complexes indicate minimal perturbation of the C^{AN}-centered LUMO energies across the series.

Photophysical Properties. The UV-vis absorption spectra and steady-state and time-resolved emission spectra of all the complexes were recorded in THF at room temperature. The overlaid UV-vis absorption spectra of complexes are depicted in Figure S4. UV-vis absorption features and assignments are very similar to other bis-cyclometalated iridium complexes from our group with the same C^{AN} ligands,^[26,27] with intense absorption bands in the UV region assigned to spin-allowed ligand-centered π→π* transitions (¹LC) involving cyclometalating and ancillary ligands, and less intense, overlapping absorption bands tailing beyond 500 nm for btp (**2a–d**) and 600 nm for piq (**1a–f**) complexes assigned as both singlet and triplet metal-to-ligand charge transfer (¹MLCT/³MLCT) transitions.

All of the complexes described here are luminescent at room temperature in deaerated THF solutions. Table 2 summarizes the steady-state and time-resolved emission data, Figures 3 and 4 show overlaid room temperature emission spectra of **1** and **2**, and the emission spectra at 77 K are displayed in Figures S15–S24. The excitation spectra of the new complexes were also collected and shown in Figures S5–S14, and in each case are superimposed with the absorption spectrum, indicating that luminescence arises solely from the iridium complex.

Our primary goal in this work is to produce complexes with improved deep-red photoluminescence attributes. The observed room-temperature emission for all of the complexes with C^{AN} = piq occurs in the deep red portion of the spectrum, with maxima

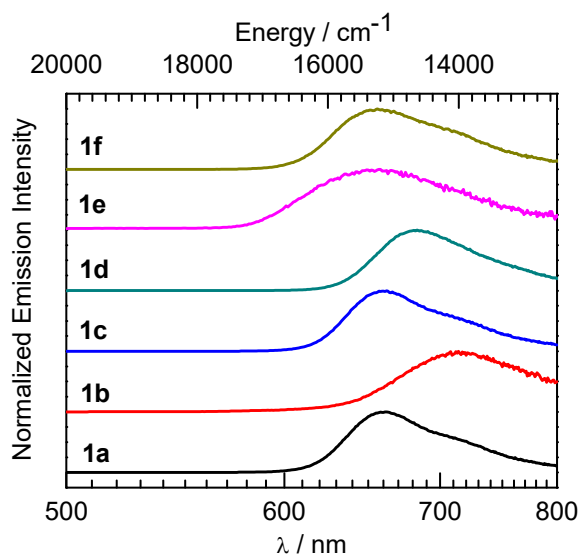


Figure 3. Overlaid emission spectra of complexes **1a–f**, were recorded in THF at room temperature. Samples were excited at λ_{exc} = 420 nm.

Table 2. Summary of photoluminescence data for all complexes

	$\lambda_{\text{max}} / \text{nm}^{[a]}$			Φ_{PL}	$\tau / \mu\text{s}$	$k_r^{[c]} \times 10^{-5} / \text{s}^{-1} / k_{\text{nr}}^{[c]} \times 10^{-5} / \text{s}^{-1}$
	THF at 293 K	Toluene at 293 K	Toluene at 77 K			
1a	660	655	642, 697	0.53	0.81	6.5/5.8
1b	707	701	666	0.071	0.90 ^[b]	0.78/10
1c	661	656	640, 699	0.58	0.74	7.8/5.6
1d	683	683	620, 678	0.37	0.53	6.8/11.8
1e	658	658	640	0.022	0.74 ^[b]	0.30/13
1f	657	655	634, 687	0.49	0.78	6.2/6.6
2a	624	622	605, 664	0.27	4.0	0.68/1.8
2b	633	627	614, 668	0.18	2.8	0.63/2.9
2c	619, 668	619, 665	609, 667	0.31	3.9 ^[b]	0.80/1.8
2d	626	626	611, 671	0.30	3.1	0.98/2.3

[a] $\lambda_{\text{exc}} = 420 \text{ nm}$. [b] Bi-exponential. Reported lifetime is a weighted average of the two time constants. [c] $k_r = \Phi/\tau$ and $k_{\text{nr}} = (1 - \Phi)/\tau$.

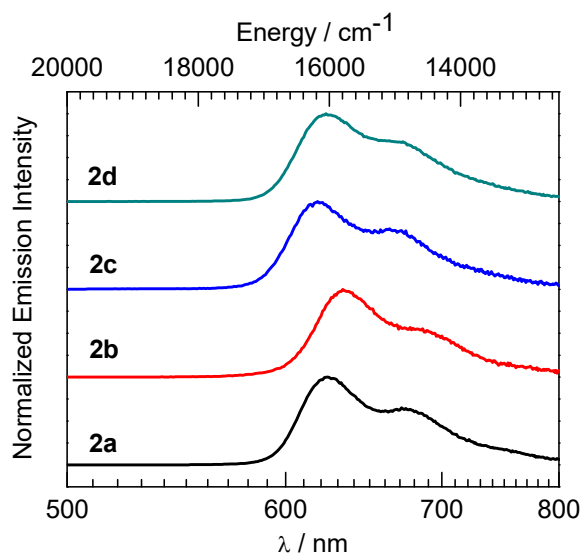


Figure 4. Overlaid emission spectra of complexes **2a–d**, were recorded in THF at room temperature. Samples were excited at $\lambda_{\text{ex}} = 420 \text{ nm}$.

beyond 650 nm that are strongly dependent on the ancillary ligand. Two key observations are noted by examining the photoluminescence data of the piq series. First, we observe that making the ancillary ligand more electron-rich red-shifts the photoluminescence, offering a potential strategy for preparing near-infrared phosphors. In piq complexes there is substantial HOMO→LUMO character in the emissive T_1 state, and CV experiments (see above) show that the HOMO energies are significantly destabilized in the more electron-rich analogues. As a result, complexes with more electron-rich ancillary ligands have smaller HOMO–LUMO gaps and red-shifted photoluminescence. For example, the previously reported complex $\text{Ir}(\text{piq})_2(\text{NacNac}^{\text{Me}})$ (**R1**)^[26] has a photoluminescence λ_{max} of 678 nm, which shifts by 29 nm (605 cm^{-1}) to 707 nm, in dimethylamino-substituted **1b**. Complex **1b** is the only compound in the series that is truly in the NIR region ($\lambda_{\text{max}} > 700 \text{ nm}$), but its modest photoluminescence quantum yield of 0.071 suggests that increasing the electron-richness of the ancillary ligand, while effective at producing NIR luminescence, may not be the best strategy for optimizing the quantum yield. Along the same lines, the complex $\text{Ir}(\text{piq})_2(\text{dipba}^{\text{Mes}})$ (**1c**) has a photoluminescence λ_{max} of 661 nm, which bathochromically shifts by 22 nm (487 cm^{-1}) in the more electron-rich dipg^{NMe2} analogue **1d**.

The more significant outcome of this study is that certain structural modifications to the ancillary ligand can lead to larger Φ_{PL} values for the deep-red emitting $\text{Ir}(\text{piq})_2(\text{L}^{\wedge}\text{X})$ complexes,

producing some of the most efficient deep-red emitters ever reported. In studying the deep-red phosphorescent compounds **R1** and **R3**, we noted modest photoluminescence quantum efficiencies on account of rather large k_{nr} values, as predicted by the energy-gap law. Our hypothesis leading into this work was that rigidifying the ancillary ligand, by adding sterically encumbering substituents, could lead to a suppression of k_{nr} and an increase in Φ_{PL} . This hypothesis was examined by preparing compounds **1a** and **1c**, more sterically crowded analogues of **R1** and **R3**. $\text{NacNac}^{\text{Me}}$ compound **R1** has a photoluminescence λ_{max} of 678 nm and a Φ_{PL} of 0.17, and in **1a** we observe a blue-shift to 660 nm, but a significant increase in quantum yield to 0.53. Similarly, dipba compound **R3** emits at 671 nm with a quantum yield of 0.34, and in **1c** the photoluminescence is mildly blue-shifted to 661 nm but the quantum yield is much higher at 0.58. The increases in quantum yield are to some extent a result of a decrease in k_{nr} , with a ca. 40% reduction in each case, but unexpectedly the more structurally rigid analogues **1a** and **1c** also exhibited larger radiative rate constants (k_r), which increased by a factor of 3.1 (**R1** to **1a**) and 1.7 (**R3** to **1c**). Thus, both an increase in k_r and a decrease in k_{nr} led to the higher quantum yields observed in sterically encumbered complexes **1a** and **1c**. We hypothesize that the slight blue-shift in complexes **1a** and **1c**, relative to **R1** and **R3**, is a result of the more sterically crowded ancillary ligand leading to a less distorted T_1 state, reducing the singlet-triplet gap. We also discovered, by preparing (Cy)acNac^{Me} complex **1f**, that incorporation of *N*-alkyl substituents onto a β -ketoiminato can also be an effective strategy for deep-red luminescence, with complex **1f** exhibiting a λ_{max} of 657 nm and a quantum yield of 0.49.

Taken together, these results not only unveiled several structure-property relationships, but also led to the discovery of a few top-performing deep-red phosphors that are significantly more efficient than previous analogues prepared by our group. We have three new compounds, **1a**, **1c**, and **1f** where the photoluminescence maximum is beyond 650 nm and the quantum yield is 0.49 or greater, and a fourth compound, **1d**, where the luminescence is very deep in the red (λ_{max} = 683 nm) and the quantum yield is still a respectable value, 0.37. These compounds all have higher quantum yields than some of the best-known deep-red phosphorescent iridium compounds in the literature. For example, $\text{Ir}(\text{C}^{\wedge}\text{N})_2(\text{acac})$ (acac = acetylacetonate) compounds where $\text{C}^{\wedge}\text{N}$ is an 8-phenylquinoline derivative, an isomer of piq, luminesce in the deep red (λ_{max} = 650–680 nm) but with a maximum Φ_{PL} of 0.11.^[34] In addition, a picolinate supported bis-cyclometalated iridium complex with $\text{C}^{\wedge}\text{N}$ = 6-phenylphenanthridine, a π -extended analogue of piq, luminesces with λ_{max} = 648 nm and Φ_{PL} = 0.27.^[35] Some recent improvements have been made by introducing new $\text{C}^{\wedge}\text{N}$ ligands, sticking exclusively with acac or picolinate-supported bis-cyclometalated iridium structures. These include an $\text{Ir}(\text{C}^{\wedge}\text{N})_2(\text{acac})$ complex with phenazine-derived $\text{C}^{\wedge}\text{N}$ ligands (λ_{max} = 684 nm and Φ_{PL} = 0.27),^[36] an $\text{Ir}(\text{C}^{\wedge}\text{N})_2(\text{acac})$ compound with spirofluorene-dibenzosuberene[d]quinoxaline $\text{C}^{\wedge}\text{N}$ ligands (λ_{max} = 686 nm and Φ_{PL} = 0.51), and finally two picolinate-supported complexes with benzo[b]thiophen-2-yl)quinoline $\text{C}^{\wedge}\text{N}$ ligands, π -extended versions of btp (λ_{max} = 651 and 661 nm, and Φ_{PL} = 0.48 and 0.37,

respectively).^[37] Clearly, there has been a surge of interest in preparing efficient deep-red iridium phosphors and applying them in optoelectronic devices, and the compounds described here offer a complementary approach to accessing deep-red emitters and have photoluminescence attributes that rival or exceed these recent breakthrough examples.

As part of this study we prepared four compounds with $\text{C}^{\wedge}\text{N}$ = btp, another cyclometalating ligand known to engender red phosphorescence. In most cases, our previous work with $\text{Ir}(\text{btp})_2(\text{L}^{\wedge}\text{X})$ compounds showed that in these compounds the photoluminescence wavelength and excited-state dynamics were not responsive to the structure of the ancillary ligand.^[26,27] A notable exception is the compound $\text{Ir}(\text{btp})_2(\text{dipba})$, which has a slightly redder photoluminescence (λ_{max} = 622 nm) and much higher quantum yield (0.79) than most other $\text{Ir}(\text{btp})_2(\text{L}^{\wedge}\text{X})$ compounds, but in almost every other case the emission wavelength was ~610 nm and the quantum yield in the narrow range of 0.2–0.3. We prepared compounds **2a–2d** to examine whether ancillary ligands which are even more sterically encumbered or even more electron rich could influence the photoluminescence in a meaningful way. But as the data in Figure 4 and Table 2 show, the photoluminescence attributes of complexes **2a–2d** are all quite similar. We do see a modest red-shift of the photoluminescence in these compounds, by 7–21 nm (185–542 cm^{-1}) relative to $\text{Ir}(\text{btp})_2(\text{acac})$,^[7] but in no case is there an increase in quantum yield. We believe this difference in behavior between piq and btp complexes arises from the larger singlet-triplet gap in the latter's $\text{C}^{\wedge}\text{N}$ ligand-centered state, leading to less excited-state MLCT character and thus less influence of the electron-rich ancillary ligand. Acknowledging that the excited-state dynamics of compounds with $\text{C}^{\wedge}\text{N}$ = btp are more difficult to influence, we believe going forward that a better strategy for continued development of deep-red and NIR emitters will be to use $\text{C}^{\wedge}\text{N}$ ligands akin to piq, where the cyclometalated aryl ring is a phenyl group and the ancillary ligand is expected to have a much more profound influence on the spectral profile and photoluminescence kinetics.

Further insight into the photoluminescence comes from low-temperature (77 K) emission spectra of the complexes. Complexes with $\text{C}^{\wedge}\text{N}$ = piq, **1a–f**, have poorly resolved vibronic structure at room temperature, but in most cases, excepting the electron-rich NacNac complexes **1b** and **1e**, two distinct vibronic maxima can be resolved at 77 K in toluene glass (Figures S15–S20). The vibronic spacing for this series of compounds falls in the range of ca. 1216–1379 cm^{-1} . Also evident in the piq series is a large rigidochromic blue-shift, which we^[17,26,27] and many others^[38] have previously noted is evidence for significant charge-transfer character in the emissive T_1 state. Better-resolved emission spectra were observed for btp complexes at 77 K, with smaller rigidochromic shifts averaging 15 nm (ca. 400 cm^{-1}) (Table 2 and Figures S21–S24). The vibronic spacing in the btp complexes is larger in most cases, at parity of ancillary ligand, and falls in the range of ca. 1316–1468 cm^{-1} .

Conclusions

We have presented here a thorough study of the effect of ancillary ligand modification on the electrochemical and optical properties of bis-cyclometalated iridium complexes, focusing in particular on the effects of electron-donating and sterically encumbering substituents. Our primary goal in this work was to improve the quantum yields of deep-red emitting complexes. Appropriate electronic tuning of the ancillary ligand in Ir(piq)₂(L^{^X}) complexes begets luminescence in the deep-red region ($\lambda_{\text{max}} > 650$ nm), and increasing the steric profile of the ancillary ligand can produce photoluminescence quantum yields >0.5 , among the highest for deep-red phosphorescence. With the most extremely electron-rich ancillary ligand NaCNac^{NMe₂} the photoluminescence is perturbed all the way to NIR region ($\lambda_{\text{max}} > 700$ nm), although the quantum yield is modest. A smaller series of compounds with C^{^N} = btp were also prepared, but in these cases the photoluminescence wavelength and the excited-state dynamics are minimally sensitive to the structure of the ancillary ligand, and only red-emitting compounds with modest quantum yields (~0.2–0.3) were produced. Taken together, these results show that our strategy of using electron-rich ancillary ligands is successful at producing some of the best-performing deep-red emitters available. Our future goals are to apply the strategy described here to significantly improve quantum yields for NIR emitters, in particular in compounds with phenyl-bound C^{^N} ligands where the excited-state dynamics are expected to be particularly sensitive to the ancillary ligand structure.

Experimental Section

Materials: Starting materials and reagents were of commercial origin and used without further purification. All reactions were executed in a nitrogen-filled glovebox operating at <1 ppm of O₂ and H₂O. Anhydrous solvents for reactions and optical measurements were dried by the method of Grubbs,^[39] passing through dual alumina columns on a commercial solvent purification system (SPS), and stored over 3 Å molecular sieves. All NMR solvents were dried and stored over 3 Å molecular sieves in the glovebox; CDCl₃ was also stored over potassium carbonate in addition to sieves. Cyclometalated iridium dimers [Ir(C^{^N})₂(μ-Cl)]₂ (C^{^N} = 1-phenylisoquinoline (piq) and 2-(2-pyridyl)benzothiophene (btp)) were prepared by the method of Nonoyama,^[40] refluxing IrCl₃·nH₂O with 2–2.3 equiv of the cyclometalating ligand in a 3:1 mixture of 2-ethoxyethanol and water. The ligand (Cy)₂NacNac^{Me}H was prepared by a literature route.^[41] Potassium or lithium salts of the acNac and NacNac ligands were prepared by the general procedure as described previously by our lab.^[17] Tetrabutylammonium hexafluorophosphate (TBAPF₆) was recrystallized from hot ethanol and ferrocene was sublimed before use in electrochemical experiments.

Physical Methods: ¹H and ¹³C{¹H} NMR spectra were recorded at room temperature using a JEOL ECA-400, ECA-500, or ECA-600 NMR spectrometer. UV-vis absorption spectra were recorded in THF solution in screw-capped quartz cuvettes using an Agilent Carey 60 UV-vis spectrophotometer. Luminescence lifetimes were measured with a Horiba DeltaFlex Lifetime System, using 390 nm pulsed diode excitation. Steady-state emission spectra were recorded using a Horiba FluoroMax-4 spectrofluorometer with appropriate long-pass filters to exclude stray excitation light from detection. In order to exclude air, samples for emission spectra were prepared in a nitrogen-filled glovebox using anhydrous solvents. Samples for room-temperature emission were housed in 1 cm

quartz cuvettes with septum-sealed screw caps, and samples for low-temperature emission were contained in a custom quartz EPR tube with high-vacuum valve and immersed in liquid nitrogen using a finger dewar. Solution quantum yields were determined relative to a standard of tetraphenylporphyrin in toluene, which has a reported fluorescence quantum yield (Φ_{PL}) of 0.11.^[42] Cyclic voltammetry (CV) measurements were performed with a CH Instruments 602E potentiostat interfaced with a nitrogen glovebox via wire feedthroughs. Samples were dissolved in acetonitrile with 0.1 M TBAPF₆ as a supporting electrolyte. A 3 mm diameter glassy-carbon working electrode, a platinum wire counter electrode, and a silver wire pseudo-reference electrode were used. Potentials were referenced to an internal standard of ferrocene.

Preparation of (Cy)acNac^{Me}H. Acetylacetone (5.00 g, 50 mmol, 1.0 equiv) and cyclohexylamine (4.46 g, 45 mmol, 0.9 equiv) were dissolved into 20 mL of DCM and the solution was stirred at room-temperature for two days. To the opaque, yellow mixture 20 mL of water were added and the organic layer was separated and dried over Na₂SO₄. The solvent was removed under reduced pressure and gave a yellow liquid. Analysis by ¹H NMR spectroscopy (Figure S25) indicated sufficient purity for further use. Yield 5.59 g (69%). ¹H-NMR (400 MHz, CDCl₃) δ : 10.97 (bs, 1H, NH), 4.89 (s, 1H, (C=O)CH(C=N)), 3.32–3.37 (m, 1H, CyH), 1.97 (s, 3H, CH₃), 1.92 (s, 3H, CH₃), 1.75–1.87 (m, 4H, Cy), 1.50–1.58 (m, 1H, Cy), 1.23–1.37 (m, 5H, Cy).

Preparation of Ir(piq)₂[(dmp)₂NacNac^{Me}] (1a). In the glovebox, [Ir(piq)₂(μ-Cl)]₂ (50 mg, 0.039 mmol) was suspended in 3 mL THF, and a solution of (dmp)₂NacNac^{Me}K (29 mg, 0.089 mmol, 2.3 equiv) in 5 mL THF was added to the dimer suspension slowly by pipet. The resulting reddish-brown mixture was stirred overnight at room temperature, during which time the color of the solution changed to dark red. The solvent was removed under reduced pressure, and the resulting residue was extracted with 5 mL of toluene and filtered through Celite to remove KCl and other insoluble impurities. The toluene was removed in vacuo, and the residue was washed with 2 × 3 mL of room-temperature Et₂O. The final product was obtained by adding pentane to a concentrated DCM solution which was dried under vacuum. Yield: 37 mg (53%). ¹H NMR (600 MHz, CDCl₃) δ : 9.23 (d, $J = 6.2$ Hz, 2H, ArH), 8.57 (d, $J = 8.9$ Hz, 2H, ArH), 7.89 (d, $J = 8.2$ Hz, 2H, ArH), 7.64–7.72 (m, 4H, ArH), 7.60 (t, $J = 7.6$ Hz, 2H, ArH), 7.42 (d, $J = 6.2$ Hz, 2H, ArH), 6.56–6.67 (m, 6H, ArH), 6.17–6.29 (m, 4H, ArH), 5.99 (d, $J = 7.6$ Hz, 2H, ArH), 4.79 (s, 1H, (Me)₂PhNC(Me)CHC(Me)NPh(Me)₂), 2.04 (s, 6H, CH₃), 1.51 (s, 6H, CH₃), 0.875 (s, 6H, CH₃). ¹³C{¹H} NMR (151 MHz, CDCl₃) δ : 171.3, 159.8, 155.2, 149.7, 146.5, 146.3, 136.8, 133.0, 132.7, 131.7, 130.5, 129.2, 128.1, 127.8, 127.5, 127.4, 127.3, 126.5, 126.4, 125.7, 122.7, 119.6, 117.5, 96.74, 25.26, 21.53, 17.02. UV-vis (THF): λ/nm ($\epsilon/\text{M}^{-1} \text{cm}^{-1}$) 302(98000), 343(sh)(50000), 390(sh)(20000), 468(21000).

Preparation of Ir(piq)₂(NacNac^{NMe₂}) (1b). In the glovebox, [Ir(piq)₂(μ-Cl)]₂ (60 mg, 0.047 mmol) was suspended in 3 mL of THF, and a solution of NacNac^{NMe₂}K (35 mg, 0.10 mmol, 2.2 equiv) in 5 mL of THF was added to the dimer suspension slowly by pipet. The resulting reddish orange mixture was stirred overnight at room temperature, during which time the color of the solution changed to dark green. The solvent was removed under reduced pressure, and the resulting residue was extracted with 5 mL of toluene and filtered through Celite to remove KCl and other insoluble impurities. The toluene was removed in vacuo, and the residue was washed with 2 × 3 mL of room-temperature Et₂O. Final product was obtained by adding pentane to a concentrated DCM solution which was dried under vacuum. Yield: 62 mg (73%). ¹H NMR (400 MHz, CDCl₃) δ : 8.73 (d, $J = 8.9$ Hz, 2H, ArH), 8.51 (d, $J = 6.9$ Hz, 2H, ArH), 8.03 (d, $J = 8.2$ Hz, 2H, ArH), 7.71 (d, $J = 8.2$ Hz, 2H, ArH), 7.47–7.58 (m, 4H, ArH), 6.96 (d, $J = 6.2$ Hz, 2H, ArH), 6.85 (t, $J = 7.6$ Hz, 2H, ArH), 6.47–6.65 (m, 8H, ArH), 6.32 (t, $J = 7.6$ Hz, 2H, ArH), 6.04 (d, $J = 8.2$ Hz, 2H, ArH), 3.83

(s, 1H, PhNC(NMe₂)CHC(NMe₂)NPh), 2.29 (s, 12H, CH₃). ¹³C{¹H} NMR (151 MHz, CDCl₃) δ: 170.1, 167.8, 162.3, 153.8, 146.2, 144.6, 136.5, 133.2, 130.2, 129.9, 128.2, 127.1, 127.0, 126.5, 126.2, 125.7, 125.6, 119.4, 119.3, 117.0, 86.17, 40.99. UV-vis (THF): λ/nm (ε/M⁻¹ cm⁻¹) 302(94000), 370(sh)(24000), 500(4000).

Preparation of Ir(piq)₂(dipba^{mes}) (1c). In the glovebox, 2-bromomesitylene (36 mg, 0.18 mmol) was dissolved in 5 mL THF and the solution was kept at -35 °C for 1 h. After that a hexane solution of *n*-BuLi (~0.11 mL, 1.6 M) was added, and the reaction mixture was stirred at -35 °C for 10 min. Then N,N'-diisopropylcarbodiimide (23 mg, 0.18 mmol) was added to the solution and the reaction mixture was stirred at room temperature for another 10 min. The colorless solution was then added dropwise to a Teflon-capped glass tube containing [Ir(piq)₂(μ-Cl)]₂ (100 mg, 0.0786 mmol) in 5 mL THF. The resulting reddish orange mixture was stirred overnight outside of glovebox at 80–85 °C, during which time the color of the solution changed to dark brown. The mixture was cooled to room temperature and the sealed tube was taken inside the glovebox for further workup procedure. The solvent was removed under reduced pressure and the residue was extracted in 2 mL toluene and evaporated under reduced pressure to remove THF completely. The product was redissolved in 10 mL toluene and filtered through Celite to remove LiCl and other insoluble impurities. The crude product was washed with 3 × 3 mL of Et₂O and 2 × 3 mL of hexane. The solid was redissolved in minimum amount of DCM and pentane was added to slowly induce precipitation and the resulted reddish-brown solid was concentrated to dryness. Yield: 55 mg (48%). ¹H NMR (600 MHz, CDCl₃) δ: 9.55 (d, *J* = 6.4 Hz, 2H, ArH), 8.96 (d, *J* = 8.2 Hz, 2H, ArH), 8.17 (d, *J* = 7.8 Hz, 2H, ArH), 7.96 (d, *J* = 7.3 Hz, 2H, ArH), 7.63–7.75 (m, 4H, ArH), 7.53 (d, *J* = 6.4 Hz, 2H, ArH), 6.77–6.93 (m, 4H, ArH), 6.61–6.67 (m, 2H, ArH), 6.36 (d, *J* = 7.8 Hz, 2H, ArH), 3.04 (sept, *J* = 6.2 Hz, 2H, (CH₃)₂CHN), 2.43 (s, 6H, CH₃), 2.25 (s, 6H, CH₃), 0.72 (d, *J* = 5.6 Hz, 6H, CH₃), -0.06 (d, *J* = 6.4 Hz, 6H, CH₃). ¹³C{¹H} NMR (151 MHz, CDCl₃) δ: 173.0, 170.1, 159.5, 146.3, 145.8, 137.2, 136.5, 136.2, 133.7, 132.6, 130.2, 129.7, 128.8, 128.3, 127.3, 127.2, 127.1, 126.2, 119.2, 119.0, 48.73, 25.17, 24.88, 21.33, 21.14. UV-vis (THF): λ/nm (ε/M⁻¹ cm⁻¹) 302(87000), 337(44000), 393(sh)(16000), 476(19000), 582(sh)(4000).

Preparation of Ir(piq)₂(dipp^{NMe2}) (1d). In the glovebox, lithium dimethylamide (~4 mg, 0.08 mmol) was dissolved in 5 mL THF and the solution was kept at -35 °C for 1 h. After that N,N'-diisopropylcarbodiimide (11 mg, 0.083 mmol) was added to the solution and the mixture was stirred at room temp for 30 min. The colorless guanidinate solution was then added dropwise to the Teflon-capped glass tube containing [Ir(piq)₂(μ-Cl)]₂ (50 mg, 0.039 mmol) in 5 mL THF. The resulting red mixture was stirred overnight outside of the glovebox at 80–85 °C, during which time the color of the solution changed to light brown. The mixture was cooled to room temperature and the sealed tube was taken inside the glovebox for further workup procedure. The solvent was removed under reduced pressure and the residue was extracted in 3 mL of toluene and evaporated under reduced pressure to remove THF completely. The product was redissolved in 5 mL of toluene and filtered through Celite to remove LiCl and other insoluble impurities. The crude product was washed with 3 × 3 mL of Et₂O and 2 × 3 mL of pentane. The crude product was redissolved in minimum amount of THF and pentane was added to the solution to slowly induced precipitation. The light brown solid was washed again with 2 × 2 mL of Et₂O and the resulting solution was concentrated to dryness. Yield: 33 mg (54%). ¹H NMR (600 MHz, CDCl₃) δ: 9.32 (d, *J* = 6.3 Hz, 2H, ArH), 8.92 (d, *J* = 8.0 Hz, 2H, ArH), 8.13 (d, *J* = 8.0 Hz, 2H, ArH), 7.93 (d, *J* = 7.4 Hz, 2H, ArH), 7.59–7.76 (m, 4H, ArH), 7.48 (d, *J* = 6.3 Hz, 2H, ArH), 6.80 (t, *J* = 7.4 Hz, 2H, ArH), 6.56 (d, *J* = 6.9 Hz, 2H, ArH), 6.22 (d, *J* = 7.4 Hz, 2H, ArH), 3.71 (sept, *J* = 6.3 Hz, 2H, (CH₃)₂CHN), 2.86 (s, 6H, CH₃), 0.57 (d, *J* = 6.3 Hz, 6H, CH₃), -0.05 (d, *J* = 6.3 Hz, 6H, CH₃). ¹³C{¹H} NMR (151 MHz, CDCl₃) δ: 170.2, 169.9, 161.2, 146.2, 143.3, 136.2, 132.6, 130.0, 129.8,

128.7, 127.2, 127.1, 126.4, 119.1, 118.9, 47.66, 40.77, 24.79, 24.33. UV-vis (THF): λ/nm (ε/M⁻¹ cm⁻¹) 305(57000), 341(sh)(31000), 464(16000), 583(sh)(4000).

Preparation of Ir(piq)₂[(Cy)₂NacNac^{Me}] (1e). In the glovebox, [Ir(piq)₂(μ-Cl)]₂ (100 mg, 0.079 mmol) was suspended in 5 mL of toluene in a Teflon-capped glass tube. A suspension of [(Cy)₂NacNac]K (45 mg, 0.15 mmol) in 5 mL of toluene was added into the tube slowly via pipette. The reaction mixture was heated outside of glovebox at 130 °C for five days. The mixture was cooled to room temperature and the sealed tube was taken inside the glovebox for further workup procedure. The resulting dark mixture was filtered through Celite and concentrated in vacuo. The residue was crystallized using 2 mL of Et₂O at -30 °C. The supernatant liquid was removed via pipette and the solid residue was washed again with 2 × 3 mL of Et₂O at -30 °C and 3 × 3 mL of pentane. The resulting solid was dried in vacuo and obtained as dark brown solid. Yield: 47 mg (37%). ¹H-NMR (500 MHz, CD₂Cl₂) δ: 9.07 (d, *J* = 6.3 Hz, 2H, ArH), 8.91 (d, *J* = 8.0 Hz, 2H, ArH), 8.14 (d, *J* = 8.0 Hz, 2H, ArH), 7.93 (d, *J* = 7.4 Hz, 2H, ArH), 7.65–7.71 (m, 4H, ArH), 7.42 (d, *J* = 6.3 Hz, 2H, ArH), 6.85 (t, *J* = 7.4 Hz, 2H, ArH), 6.56 (t, *J* = 7.2 Hz, 2H, ArH), 4.00 (s, 1H, CyNC(Me)CHC(Me)NCy), 2.97 (t, *J* = 11.5 Hz, 2H, CyH), 1.89 (s, 6H, CH₃), 1.59–1.63 (m, 4H, Cy), 1.12–1.32 (m, 6H, Cy), 0.90–0.99 (m, 2H, Cy), 0.63–0.71 (m, 2H, Cy), 0.50–0.54 (m, 2H, Cy), 0.30–0.40 (m, 2H, Cy), 0.01–0.07 (m, 2H, Cy). ¹³C{¹H} NMR (126 MHz, CD₂Cl₂) δ: 169.67, 162.76, 158.34, 146.51, 144.38, 136.82, 132.25, 130.37, 129.74, 128.65, 127.22, 126.99, 126.91, 126.35, 119.38, 118.51, 99.84, 66.35, 34.41, 33.75, 26.94, 26.30, 26.09, 24.88. UV-vis (THF): λ/nm (ε/M⁻¹ cm⁻¹) 299 (38000), 405(17000), 533(sh)(12000).

Preparation of Ir(piq)₂[(Cy)acNac^{Me}] (1f). In the glovebox, [Ir(piq)₂(μ-Cl)]₂ (100 mg, 0.079 mmol) was suspended in 5 mL of toluene in a Teflon-capped glass tube. A suspension of (Cy)acNac^{Me}K (33 mg, 0.15 mmol) in 5 mL of toluene was added into the tube slowly via pipette. The reaction mixture was heated outside of glovebox at 130 °C for five days. The mixture was cooled to room temperature and the sealed tube was taken inside the glovebox for further workup procedure. The resulting dark red mixture was filtered through Celite and concentrated in vacuo. The residue was crystallized using 2 mL of Et₂O at -35 °C. The supernatant liquid was removed via pipette and the solid residue was washed again with 2 × 3 mL of cold Et₂O and 3 × 3 mL of pentane. The resulting solid was dried in vacuo and obtained as dark red solid. Yield: 41 mg (35%). ¹H-NMR (400 MHz, CD₂Cl₂) δ: 8.98–9.04 (m, 1H, ArH), 8.92 (d, *J* = 7.8 Hz, 1H, ArH), 8.75 (q, *J* = 6.6 Hz, 2H, ArH), 8.30 (d, *J* = 8.2 Hz, 1H, ArH), 8.15 (d, *J* = 7.8 Hz, 1H, ArH), 7.92–7.99 (m, 2H, ArH), 7.66–7.75 (m, 4H, ArH), 7.48 (dd, *J* = 6.4, 2.9 Hz, 2H, ArH), 6.91 (q, *J* = 7.2 Hz, 2H, ArH), 6.58–6.70 (m, 2H, ArH), 6.45 (d, *J* = 7.8 Hz, 1H, ArH), 6.19 (d, *J* = 6.9 Hz, 1H, ArH), 4.56 (s, 1H, CyNC(Me)CHC(O)Me), 3.06 (s, 1H, CyH), 1.99 (s, 3H, CH₃), 1.59 (s, 3H, CH₃), 0.96–1.43 (m, 5H, Cy), 0.60–0.92 (m, 1H, Cy), 0.01–0.48 (m, 3H, Cy). ¹³C{¹H} NMR (126 MHz, CD₂Cl₂) δ: 173.73, 169.38, 168.70, 163.12, 158.47, 157.57, 147.01, 146.22, 142.97, 141.42, 137.03, 136.89, 133.16, 132.33, 130.59, 130.56, 130.34, 129.63, 129.07, 128.30, 127.75, 127.52, 127.04, 126.94, 126.46, 126.41, 126.32, 120.55, 119.83, 119.37, 99.77, 66.07, 32.40, 31.97, 26.51, 26.21, 25.73. UV-vis (THF): λ/nm (ε/M⁻¹ cm⁻¹) 298(36000), 322(sh)(23000), 384(sh)(11000), 486(5300).

Preparation of Ir(btp)₂[(dmp)₂NacNac^{Me}] (2a). Prepared by the method described above for complex **1a**, using [Ir(btp)₂(μ-Cl)]₂ (50 mg, 0.038 mmol) and (dmp)₂NacNac^{Me}K (30 mg, 0.089 mmol). The purified product was a dark orange colored solid. Yield: 43 mg (63%). ¹H NMR (600 MHz, CDCl₃) δ: 9.24 (d, *J* = 6.2 Hz, 2H, ArH), 7.70 (t, *J* = 7.6 Hz, 2H, ArH), 7.33 (d, *J* = 7.6 Hz, 2H, ArH), 7.27 (d, *J* = 7.6 Hz, 2H, ArH), 7.03 (t, *J* = 6.2 Hz, 2H, ArH), 6.86 (t, *J* = 6.9 Hz, 2H, ArH), 6.57 (t, *J* = 7.6 Hz, 2H, ArH), 6.38–6.47 (m, 4H, ArH), 5.95 (d, *J* = 6.9 Hz, 2H, ArH), 5.90 (d, *J* = 8.3 Hz, 2H, ArH), 4.79 (s, 1H, (Me)₂PhNC(Me)CHC(Me)NPh(Me)₂), 1.82 (s, 6H, CH₃),

1.68 (s, 6H, CH₃), 1.32 (s, 6H, CH₃). ¹³C{¹H} NMR (151 MHz, CDCl₃): 167.5, 159.2, 155.0, 152.5, 148.5, 146.1, 142.4, 137.6, 136.0, 133.0, 132.6, 127.4, 126.9, 126.0, 124.0, 123.4, 122.2, 122.0, 117.5, 117.4, 98.08, 25.61, 23.88, 17.53. UV-vis (THF): λ/nm (ε/M⁻¹ cm⁻¹) 297(51000), 332(36000), 359(33000), 383(sh)(32000), 498(sh)(5000).

Preparation of Ir(btp)₂(NacNac^{NMe2}) (2b). Prepared by the method described above for complex **1b**, using [Ir(btp)₂(μ-Cl)₂] (50 mg, 0.038 mmol) and (dmp)₂NacNac^{NMe2}K (27 mg, 0.078 mmol, 2.1 equiv). The purified product was a light orange colored solid. Yield: 35 mg (50%). ¹H NMR (400 MHz, CDCl₃) δ: 8.75 (d, *J* = 5.5 Hz, 2H, ArH), 7.60 (d, *J* = 8.2 Hz, 2H, ArH), 7.43 (t, *J* = 6.9 Hz, 2H, ArH), 7.13–7.17 (m, 2H, ArH), 6.99 (t, *J* = 8.2 Hz, 2H, ArH), 6.66–6.76 (m, 4H, ArH), 6.44–6.58 (m, 6H, ArH), 6.09 (d, *J* = 8.2 Hz, 2H, ArH), 5.96 (d, *J* = 7.6 Hz, 4H, ArH), 4.06 (s, 1H, PhNC(NMe₂)CHC(NMe₂)NPh), 2.38 (s, 12H, CH₃). ¹³C{¹H} NMR (151 MHz, CDCl₃) δ: 167.1, 166.7, 155.4, 152.4, 151.1, 147.4, 142.5, 136.7, 135.0, 129.1, 128.3, 127.1, 126.3, 126.1, 124.4, 123.2, 122.5, 119.6, 117.2, 116.9, 84.61, 41.21. UV-vis (THF): λ/nm (ε/M⁻¹ cm⁻¹) 296(58000), 370(sh)(24000), 500(4000).

Preparation of Ir(btp)₂(dipba^{NMe2}) (2c). In the glovebox, 2-bromomesitylene (~33 mg, 0.17 mmol) was dissolved in 5 mL THF and the solution was kept at -35 °C for 1 h. After that a hexane solution of *n*-BuLi (~0.11 mL, 1.6 M) was added, and the reaction mixture was stirred at -35 °C for 10 min. Then N,N'-diisopropylcarbodiimide (~21 mg, 0.17 mmol) was added to the solution and the reaction mixture was stirred at room temp for 10 min. The colorless solution was then added dropwise to the Teflon-capped glass tube containing [Ir(btp)₂(μ-Cl)₂] (100 mg, 0.0769 mmol) in 5 mL of THF. The resulting yellow mixture was stirred overnight outside of glovebox at 80–85 °C, during which time the color of the solution changed to light orange. The mixture was cooled to room temperature and the sealed tube was taken inside the glovebox for further workup procedure. The solvent was removed under reduced pressure and the residue was extracted into 3 mL of toluene and evaporated under reduced pressure to remove THF completely. The product was redissolved in 15 mL of toluene and filtered through Celite to remove LiCl and other insoluble impurities. The crude product was washed with 3 × 3 mL of Et₂O and 2 × 3 of mL hexane. The solid was redissolved in minimum amount of DCM and pentane was added to slowly induce precipitation and the resulted orange solid was concentrated to dryness. Yield: 42 mg (32%). ¹H NMR (600 MHz, CDCl₃) δ: 9.52 (d, *J* = 5.5 Hz, 2H, ArH), 7.77 (t, *J* = 7.9 Hz, 2H, ArH), 7.63 (dd, *J* = 7.6, 35 Hz, 4H, ArH), 7.01–7.11 (m, 4H, ArH), 6.76–6.88 (m, 4H, ArH), 6.21 (d, *J* = 8.2 Hz, 2H, ArH), 2.96 (sept, *J* = 6.2 Hz, 2H, (CH₃)₂CHN), 2.37 (s, 6H, CH₃), 2.25 (s, 6H, CH₃), 0.59 (d, *J* = 6.2 Hz, 6H, CH₃), 0.07 (d, *J* = 6.2 Hz, 6H, CH₃). ¹³C{¹H} NMR (151 MHz, CDCl₃) δ: 174.3, 167.1, 154.4, 153.5, 147.6, 142.7, 137.7, 136.9, 136.0, 134.5, 132.7, 128.6, 126.0, 124.7, 123.4, 122.7, 117.4, 117.6, 48.08, 24.75, 24.55, 21.54, 21.15. UV-vis (THF): λ/nm (ε/M⁻¹ cm⁻¹) 288(64000), 331(40000), 432(13000), 486(sh)(8000), 583(sh)(1000).

Preparation of Ir(btp)₂(dipg^{NMe2}) (2d). Prepared by the method described above for complex **1d**, using [Ir(btp)₂(μ-Cl)₂] (100 mg, 0.0768 mmol), lithium dimethylamide (~8 mg, 0.16 mmol, 2.1 equiv), and N,N'-diisopropylcarbodiimide (~20 mg, 0.16 mmol). The purified product was a light orange colored solid. Yield: 61 mg (51%). ¹H NMR (600 MHz, CDCl₃) δ: 9.26 (d, *J* = 5.5 Hz, 2H, ArH), 7.58 (dd, *J* = 8.3, 33 Hz, 4H, ArH), 6.97–7.07 (m, 4H, ArH), 6.76 (t, *J* = 7.6 Hz, 2H, ArH), 6.16 (d, *J* = 7.6 Hz, 2H, ArH), 3.60 (septa, *J* = 6.2 Hz, 2H, (CH₃)₂CHN), 2.80 (s, 6H, CH₃), 0.47 (d, *J* = 6.2 Hz, 6H, CH₃), 0.01 (d, *J* = 6.2 Hz, 6H, CH₃). ¹³C{¹H} NMR (151 MHz, CDCl₃) δ: 170.6, 167.2, 151.6, 147.6, 145.5, 142.7, 136.2, 133.6, 125.9, 124.6, 123.2, 122.5, 118.0, 117.7, 47.0, 40.6, 24.2, 24.0. UV-vis (THF): λ/nm (ε/M⁻¹ cm⁻¹) 334(48000), 427(19000), 517(10000), 595(sh)(2000).

X-ray Crystallography Details: Single crystals were grown by vapor diffusion of pentane vapor into concentrated THF or dichloromethane solutions. Crystals were mounted on a Bruker Apex II three-circle diffractometer using MoKα radiation (λ=0.71073 Å). The data was collected at 123(2) K and was processed and refined within the APEXII software. Structures were solved by direct methods in SHELXS and refined by standard difference Fourier techniques in the program SHELXL.^[43] Hydrogen atoms were placed in calculated positions using the standard riding model and refined isotropically; all non-hydrogen atoms were refined anisotropically.

Acknowledgements

The authors acknowledge the National Science Foundation (CHE-1846831) and the Welch Foundation (grant no. E-1887) for funding this research. B.-L. N. acknowledges the University of Houston for an undergraduate research fellowship through the SURF program.

Conflicts of interest

The authors declare no conflict of interest.

Keywords: red-emitting • cyclometalated iridium • cyclic voltammetry • ligand modification • luminescence

- [1] C. K. Prier, D. A. Rankic, D. W. C. MacMillan, *Chem. Rev.* **2013**, *113*, 5322–5363.
- [2] Z. Zuo, D. T. Ahneman, L. Chu, J. A. Terrett, A. G. Doyle, D. W. C. MacMillan, *Science* **2014**, *345*, 437–440.
- [3] T. P. Yoon, M. A. Ischay, J. Du, *Nat. Chem. Lond.* **2010**, *2*, 527–32.
- [4] Q. Zhao, F. Li, S. Liu, M. Yu, Z. Liu, T. Yi, C. Huang, *Inorg. Chem.* **2008**, *47*, 9256–9264.
- [5] Q. Zhao, F. Li, C. Huang, *Chem. Soc. Rev.* **2010**, *39*, 3007–3030.
- [6] H. (Hartmut) Yersin, *Highly Efficient OLEDs with Phosphorescent Materials*, Weinheim: Wiley-VCH, **2008**.
- [7] S. Lamansky, P. Djurovich, D. Murphy, F. Abdel-Razzaq, H.-E. Lee, C. Adachi, P. E. Burrows, S. R. Forrest, M. E. Thompson, *J. Am. Chem. Soc.* **2001**, *123*, 4304–4312.
- [8] M. S. Lowry, S. Bernhard, *Chem. – Eur. J.* **2006**, *12*, 7970–7977.
- [9] M. Sarma, W.-L. Tsai, W.-K. Lee, Y. Chi, C.-C. Wu, S.-H. Liu, P.-T. Chou, K.-T. Wong, *Chem* **2017**, *3*, 461–476.
- [10] R. D. Costa, E. Ortí, H. J. Bolink, F. Monti, G. Accorsi, N. Armadori, *Angew. Chem. Int. Ed.* **2012**, *51*, 8178–8211.
- [11] T.-B. Gao, J.-J. Zhang, R.-Q. Yan, D.-K. Cao, D. Jiang, D. Ye, *Inorg. Chem.* **2018**, *57*, 4310–4316.
- [12] K. Dedeian, P. I. Djurovich, F. O. Garces, G. Carlson, R. J. Watts, *Inorg. Chem.* **1991**, *30*, 1685–1687.
- [13] A. B. Tamayo, B. D. Alleyne, P. I. Djurovich, S. Lamansky, I. Tsyba, N. Ho, R. Bau, M. E. Thompson, *J. Am. Chem. Soc.* **2003**, *125*, 7377–7387.
- [14] Y. You, S. Y. Park, *J. Am. Chem. Soc.* **2005**, *127*, 12438–12439.
- [15] C.-J. Chang, C.-H. Yang, K. Chen, Y. Chi, C.-F. Shu, M.-L. Ho, Y.-S. Yeh, P.-T. Chou, *Dalton Trans.* **2007**, 1881–1890.
- [16] J. Li, P. I. Djurovich, B. D. Alleyne, M. Yousufuddin, N. N. Ho, J. C. Thomas, J. C. Peters, R. Bau, M. E. Thompson, *Inorg. Chem.* **2005**, *44*, 1713–1727.
- [17] Y. K. Radwan, A. Maity, T. S. Teets, *Inorg. Chem.* **2015**, *54*, 7122–7131.
- [18] Md. K. Nazeeruddin, R. Humphry-Baker, D. Berner, S. Rivier, L. Zuppiroli, M. Graetzel, *J. Am. Chem. Soc.* **2003**, *125*, 8790–8797.
- [19] T. Sajoto, P. I. Djurovich, A. B. Tamayo, J. Oxgaard, W. A. Goddard, M. E. Thompson, *J. Am. Chem. Soc.* **2009**, *131*, 9813–9822.
- [20] C.-H. Yang, M. Mauro, F. Polo, S. Watanabe, I. Muenster, R. Fröhlich, L. De Cola, *Chem. Mater.* **2012**, *24*, 3684–3695.

-
- [21] N. M. Shavaleev, F. Monti, R. D. Costa, R. Scopelliti, H. J. Bolink, E. Ortí, G. Accorsi, N. Armaroli, E. Baranoff, M. Grätzel, M. K. Nazeeruddin, *Inorg. Chem.* **2012**, *51*, 2263–2271.
- [22] S. Haneder, E. D. Como, J. Feldmann, J. M. Lupton, C. Lennartz, P. Erk, E. Fuchs, O. Molt, I. Münster, C. Schildknecht, G. Wagenblast, *Adv. Mater.* **2008**, *20*, 3325–3330.
- [23] M. Bixon, J. Jortner, *J. Chem. Phys.* **1968**, *48*, 715–726.
- [24] R. Englman, J. Jortner, *Mol. Phys.* **1970**, *18*, 145–164.
- [25] S. D. Cummings, R. Eisenberg, *J. Am. Chem. Soc.* **1996**, *118*, 1949–1960.
- [26] P.-N. Lai, C. H. Brysacz, M. K. Alam, N. A. Ayoub, T. G. Gray, J. Bao, T. S. Teets, *J. Am. Chem. Soc.* **2018**, *140*, 10198–10207.
- [27] P.-N. Lai, T. S. Teets, *Chem. – Eur. J.* **2019**, *25*, 6026–6037.
- [28] J.-H. Shon, T. S. Teets, *Inorg. Chem.* **2017**, *56*, 15295–15303.
- [29] J.-H. Shon, S. Sittel, T. S. Teets, *ACS Catal.* **2019**, *9*, 8646–8658.
- [30] Y. Liu, K. Ye, Y. Fan, W. Song, Y. Wang, Z. Hou, *Chem. Commun.* **2009**, 3699–3701.
- [31] Z.-T. Yu, Y.-J. Yuan, J.-G. Cai, Z.-G. Zou, *Chem. – Eur. J.* **2013**, *19*, 1303–1310.
- [32] V. K. Rai, M. Nishiura, M. Takimoto, Z. Hou, *J. Mater. Chem. C* **2014**, *2*, 5317–5326.
- [33] R. A. Maya, A. Maity, T. S. Teets, *Organometallics* **2016**, *35*, 2890–2899.
- [34] H.-C. Li, P.-T. Chou, Y.-H. Hu, Y.-M. Cheng, R.-S. Liu, *Organometallics* **2005**, *24*, 1329–1335.
- [35] J. M. Fernandez-Hernandez, E. Longhi, R. Cysewski, F. Polo, H.-P. Josel, L. De Cola, *Anal. Chem.* **2016**, *88*, 4174–4178.
- [36] C. You, D. Liu, F. Meng, Y. Wang, J. Yu, S. Wang, S. Su, W. Zhu, *J. Mater. Chem. C* **2019**, *7*, 10961–10971.
- [37] H. U. Kim, H. J. Jang, W. Choi, M. Kim, S. Park, T. Park, J. Y. Lee, B. K. S., *J. Mater. Chem. C* **2019**, *7*, 4143–4154.
- [38] A. J. Lees, *Comments Inorg. Chem.* **1995**, *17*, 319–346.
- [39] A. B. Pangborn, M. A. Giardello, R. H. Grubbs, R. K. Rosen, F. J. Timmers, *Organometallics* **1996**, *15*, 1518–1520.
- [40] M. Nonoyama, *Bull. Chem. Soc. Jpn.* **1974**, *47*, 767–768.
- [41] I. El-Zoghbi, S. Latreche, F. Schaper, *Organometallics* **2010**, *29*, 1551–1559.
- [42] P. G. Seybold, M. Gouterman, *J. Mol. Spectrosc.* **1969**, *31*, 1–13.
- [43] G. M. Sheldrick, *Acta Crystallogr. A* **2008**, *64*, 112–122.
-